Nanoscale

ARTICLE

Nanoscale Accepted Manuscript

Immunogold Labeling Reveals Subcellular Localisation of Silica Nanoparticles in a Human Blood-Brain Barrier Model

Dong Ye,[1] Sergio Anguissola,[1] Tiina O'Neill,[2] Kenneth A. Dawson[1*]

Subcellular location of nanoparticles has been widely investigated with fluorescence microscopy, *via* fluorescently labeled antibodies to visualise target antigens in cells. However, fluorescence microscopy, such as confocal or live cell imaging, have generally limited 3D spatial resolution. Conventional electron microscopy can be useful in bridging resolution gap, but still not ideal in resolving subcellular organllel identities. Using the pre-embedding immunogold electron microscopic imaging, we performed accurate examination of the intracellular trafficking and gathered further evidence of transport mechanisms of silica nanoparticles across a human *in vitro* blood-brain barrier model. Our approach can effectively immunolocalise a variety of intracellular compartments and provide new insights into the uptake and subcellular transport of nanoparticles.

Introduction

Identifying molecular components of subcellular compartments is crucial for investigating structural and physiological properties of cells. Currently significant efforts have been directed to investigate membrane trafficking regulation in order to dissect cellular transport pathways, mainly this was achieved by using light microscopy approaches (LM).[1] [2] Confocal or live-cell imaging, for example, can provide a non-invasive and real-time analysis by tracking co-localisation of nanoparticles and subcellular compartments by exploiting overlap fluorescence patterns. However, conventional confocal microscopy reaches a lateral spatial resolution of 200-300 nm and an axial resolution of 500-700 nm.[3, 4] Such resolution is sufficient for visualisation of certain cellular organelles, such as nucleus, Golgi, mitochondria, etc.,[5] but insufficient for identification of smaller objects, such as single endocytic vesicles or their interactive entities, particularly nanoparticles that are below 100 nm. The advent of the era of super resolution fluorescence microscopy, such as STORM and PALM, or optical nanoscopy, has seen big advance in overcoming diffraction limits,[6-8] but still these techniques are limited to objects with fluorescence labels.

Immunogold (IG) labeling exploits colloidal gold particles attached to a secondary antibody as counterstain for electron microscopic imaing to reveal specific protein markers of subcellular organelles detected by a specific primary antibody. With high electron density as well as accurate immunorecognition, IG particles provide easy detection for intracellular components or structures under transmission electron micoscopy (TEM). Two types of IG labeling methods, the post-embedding and pre-embedding labeling have been discussed in literature.[9-11] Although the post-embedding IG labeling enables direct detection of antigens from sections, preparation of these samples usually requires cryogenic processing in order to preserve antigen specificity, which does not allow for prolonged IG labeling and satisfactory signal-to-noise ratio.[12] On the contrary, pre-embedding IG labeling, which is performed similar to immunofluorescence staining does not need cryogenic processing or freeze substitution. The staining procedure involves a permeablisation step followed by primary antibody and secondary nanogold-antibody conjugate staining, sample embedding and subsequently ultramicrotomic sectioning. Although pre-embedding labeling was reportedly subject to poor performance from IG probes, recently, 1.4 nm colloidal nanogold-Fab' or IgG conjugates have been commercially developed to attain optimal penetration and labeling quality in cells and tissues.[13, 14] In addtion, siliver enhancement is commonly applied after the immunolabeling to improve electron beam detection. This technique uses the gold nanoparticles for silver nucleation, allowing to enlarge 1.4 nm nanogolds up to several tens of nanometers generating significantly enhanced detection under TEM.[11, 15] Moreover, nanogold probes can be tailored by crosslinking secondary antibodies coupled with choices of fluorophores, allowing to investigate biological specimens with both light and electron microscopic imaging, known as correlative light and electron microscopy (CLEM).[16, 17]

Nanometerials have been extensively studied as diagnostic imaging agents, drug-carriers and therapeutic agents. The modalities of internalisation of nanoparticles by cells or tissues play a key role in exerting the desired activity of nanoparticles, for instance, targeted access of nanomedicines to tumor cells for cancer treatment.[18] Many epithelial or endothelial cells have been found to internalise nanoparticles, depending on concentration, time, size, surface properties, biomolecular corona composition, cell cycle or even cell types.[19-25] Nanoparticles are trafficked inside cells via associated subcellular membrane-enclosed structures following the endo-lysosomal pathway.[1, 23, 26] Characterising interactions of nanoparticles with cellular organelles at morphological level is not trivial, particularly considering nanomaterials' physico-chemical conditions and aggregation state. As a valuable approach, TEM can reliably multitask our needs in both qualitative and quantitative imaging studies at nanoscales. Direct quantiation in TEM will further qualitative imaging analysis into understanding the dynamics of nanoparticles in cells and faciliate calibration of indirect measurement techniques such as integrated fluorescence. This field has been reviewed and implemented with a stereological approach in TEM by Elasesser *et al.*[27, 28] In addition, it is noteworthy that IG labeling electron microscopy has been rarely applied to investigate subcellular translocation of nanoparticles, its value to understand biological components that mediate nanoparticle transport, is underrated, especially in biological barriers such as the blood-brain barrier (BBB).

Previously, we reported that trafficking of nanoparticles in the BBB utilised clathrin or caveolin-mediated endocytosis, the endo-lysosomal pathway, and their potential export was observed via transcytosis by immunofluorescence light microscopy and conventional electron microscopy.[2, 26] Specific membrane-enclosed compartments, such as endosomes or lysosomes, can be distinguished according to their electron densities and morphologies. However, when these vesicles evolve along the endo-lysosomal pathway, they may undergo biological changes (e.g. pH), which may influence morphology-based judgement and cause incorrect identitification of membrane-bound structures under TEM. Accurate IG labeling is a superior approach to identify subcellular entities that mediate nanoparticle trafficking. By performing immunolabeling of Rab GTPase proteins, known to control the identities of vescicles along the endo-lysosomal pathway and regulate delivery of cargos between subcellular organelles,[29] we characterised sorting and routing mechanisms of nanoparticles at high spatial and temporal resolution. Moreover, distinct primary antibodies for clathrin, caveolin, EEA 1 and LAMP 1 were also applied to dissect trafficking of nanoparticles in the BBB.

Results and discussion

It was previously reported that chemical permeablisation performed prior to the resin embedding might alter cellular ultrastructures, leading to low quality immunocytochemical preservation.[30] A periodate-lysine-paraformaldehyde fixative, which was proven suitable to retain antigenicity and stabilise cellular structures,[31] was therefore used in this report. In addition, we found glutaraldehyde could improve the preservation of cell membrane as well as other intracellular organelles (Supplementary Figure 1) following the membrane permeabilisation and fixation, as found previously.[32]

In our cell culture, hCMEC/D3 cells acquired an endothelial phenotype, in which they could form cell-to-cell tight junctions and display apical-basal polarity via membrane-segregated protein complexes. Previously, we developed a method to acquire apical-to-basal transversal sections from the BBB cell layer using ultramicrotomic sectioning.[26, 33] The 2D images projected by this TEM approach were analogous to a perpendicular plane, *xz* or *yz*, projected in confocal microscopy.[1, 2, 26] As a result, sectioning the BBB with prior staining of colloidal nanogold immunoprobes would empower TEM to identify subcellular structures along routing pathways for nanoparticles across a polarised BBB cell layer. Precision of the IG labeling could be exemplified by staining results from anti-LAMP 1 and EEA 1 in Supplementary Figure 1&3. To confirm the specificity of labeling, the BBB cells incubated with only secondary nanogold-antibody conjugates were imaged in Supplementary Figure 2.

The BBB cell barriers were exposed to 50 nm SiO_2-NPs for various times. Physiochemical characterisation of silica nanoparticles was provided in Supplementary Table 1. A panel of primary antibodies (for Clathrin, Caveolin 1, LAMP 1, EEA 1, Rab 5, 7 and 11) used in combination with 1.4 nm nanogold-Fab' fragment secondary IgG, were applied using our pre-embedding immunostaining procedures. All samples were stained with an equal concentration of primary and secondary antibodies, in order to compare the immunoreactivity between each type of primary antibody and its target antigen. After staining with 1.4 nm nanogold probes, samples were processed for silver enhancement, which could initiate self-nucleation of gold nanoparticles in a time-dependent manner.[11, 15] In Supplementary Figure 3, silver-enhancing reagents were applied to the cell barriers stained with the lysosomal marker LAMP 1 and subsequently counterstained with the immunogold probe. The silver enhancement was performed at 0, 1, 2, 4, 5 and 7 min respectively, in order to compare the size increment of nanogold particles. As seen in the results, 1.4 nm IG particles were effectively enlarged up to tens of nanometres after 5-7 min, and their identification was significantly improved as a result of increased sizes.
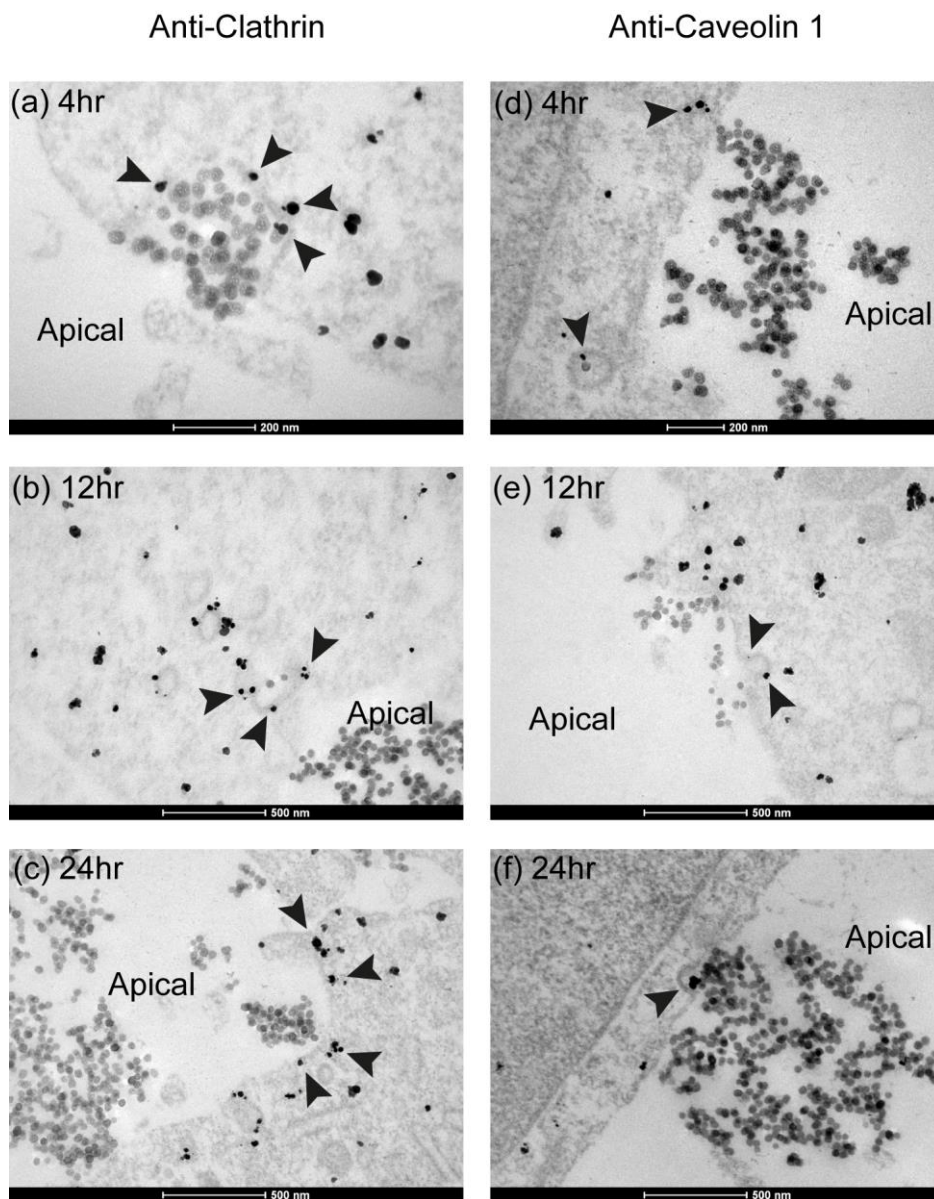
Nanoscale Accepted Manuscript

Figure 1. IG detection of clathrin and non-clathrin mediated endocytosis on the apical membrane of the BBB following exposure to 50 nm SiO_2-NPs for 4, 12 and 24 hours. Clathrin (a, b, c) and caveolin 1 (d, e, f)-containing vesicular structures were associated with silica nanoparticles and detected with IG staining, as indicated by the black arrows.

The cell membrane is the biological interface that initiates cell machinery for uptake of nanoparticles. To study early endocytosis, anti-clathrin and anti-caveolin 1 primary antibodies were used to investigate clathrin- and caveolin-dependent endocytic processes. Clathrin is known to assemble cell membrane structures that mediate uptake by early endocytosis.[34] On the other hand, caveolin, a component of caveolae, form clathrin-independent membrane invaginations that function as carriers during caveolar endocytosis.[34, 35] As observed in Fig. 1a-c, 50 nm SiO_2-NPs were internalised by the apical membrane of endothelial cells *via* flask-shaped vesicles after 4, 12 and 24 hours of exposure. The vesicles that were positively immunodetected for clathrin showed distinct dimensions, which varied according to the agglomerated (Fig.

1a, c) or single (Fig. 1b) nanoparticles during their uptake. Moreover, caveolin-mediated (or non-clathrin dependent) vesicular endocytosis was also observed. A single nanoparticle was first observed to be internalised within a caveola by immunogold detection for caveolin-1 (Fig. 1d). In Fig. 1e-f, the electron micrographs described several caveolae invaginations were approached by both single and agglomerated SiO_2-NPs on the apical membrane of the BBB. Since the access of nanoparticles to caveolar cavities was reportedly limited by the size of a caveola (approx. 60-80 nm),[36] so agglomerated 50 nm SiO_2-NPs were potentially unable to be taken up through caveolae-mediated endocytosis.
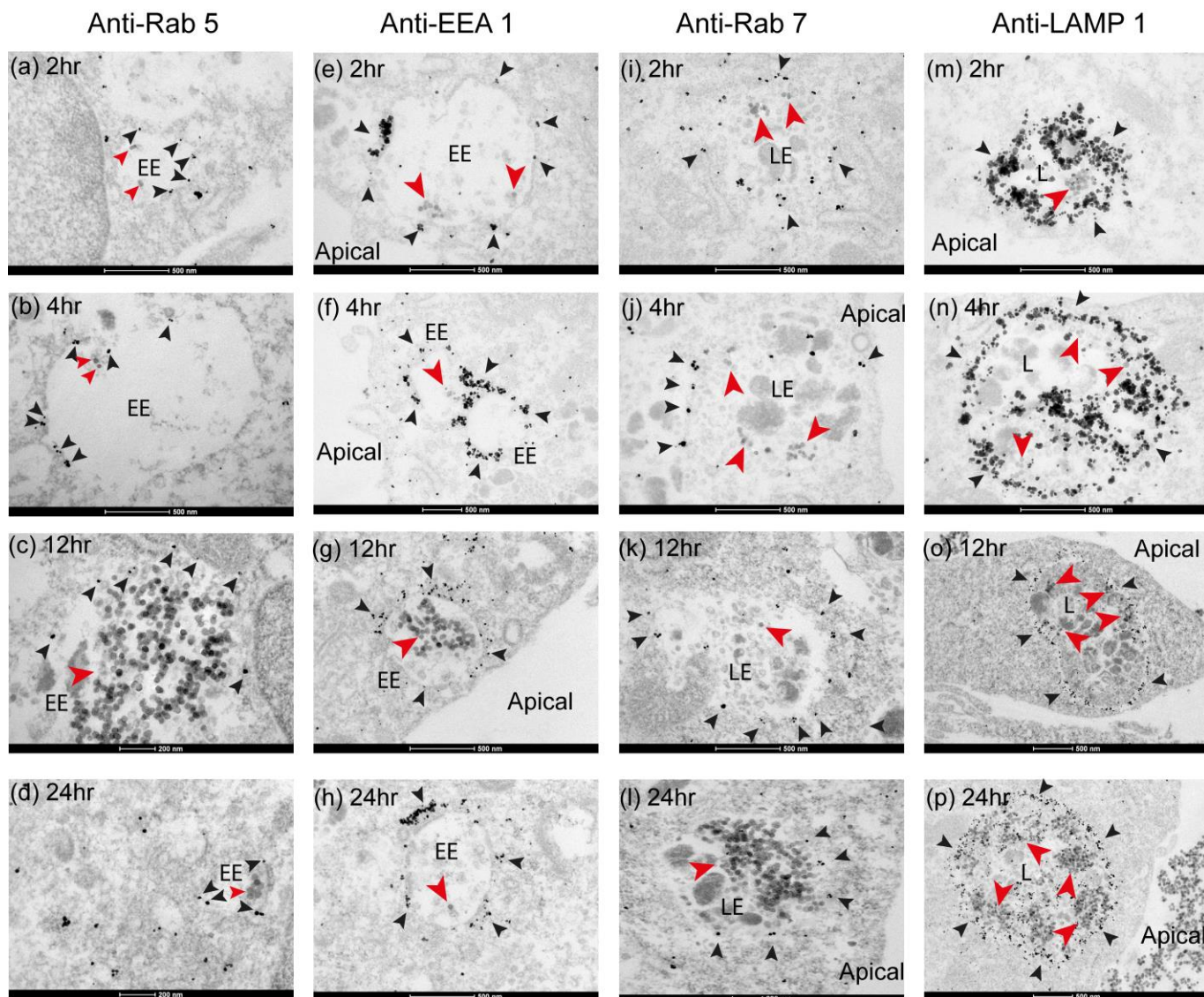
Figure 2. Nanogold immunolocalisation of subcellular organelles stained with Rab 5, EEA 1, Rab 7 or LAMP 1 antibody respectively after exposure of 50 nm SiO$_2$-NPs to the BBB for 2, 4, 12 and 24 hours. The black arrows indicated immunolocalised nanogold probes; the red arrows represented the 50 nm SiO$_2$-NPs co-localised with subcellular compartments. EE, early endosomes; LE, late endosomes; L, lysosomes.

Further, SiO$_2$-NPs were transferred to endosomal compartments, for either degradation or recycling.[29, 37, 38] Identification of endosomal structures was difficult, as they differed at individual maturation stages. Here, we used several antibodies to target a variety of markers (including EEA 1, LAMP 1 and Rab proteins) to distinguish endosomes and lysosomes. As shown by the distribution of antibodies-labelled IG in Fig. 2, 50 nm SiO$_2$-NPs co-localised both endosomes and lysosomes. Rab 5 and EEA 1 were both membrane constituents of early endosomes, each of which was seen with less electron density compared to lysosomes (Fig. 2a-d and e-h). The silver and gold colloidal grains deposited at the endosomal and lysosomal membrane borders. SiO$_2$-NPs were internalised by endosomes and lysosomes throughout all exposure times. The IG staining results from Rab 5 and EEA 1 were very different, which might be influenced by either the immunoreactivities of Rab 5 and EEA 1 antibodies with their antigens or their expression levels on the endosomal membrane.

Along the pathway of maturation from endosomes to lysosomes, late endosomes were normally enriched with sorting vesicles, which resulted in their multivesicular appearance and intermediated electron density. Late endosomes were identified with the endosomal regulator Rab 7 (Fig. 2i-l). After 24-hour incubation, SiO$_2$-NPs showed accumulation in late endosomes. Similar to Rab 5, immunostaining of Rab 7 did not show a large number of labels of IG particles compared with EEA 1, suggesting less efficient immunoreaction with the Rab 7 antigens. Some endosomal membranes did not always show clear boundary (Fig. 2a-d and 2i-l), which might be caused by the high contrast of silver and gold colloidal grains localised nearby. Staining with the lysosomal marker, LAMP 1, we further demonstrated time-dependent co-localizations of SiO$_2$ nanoparticles in lysosomes (Fig. 2m-p). IG particles specifically targeted the membrane-enclosed lysosomal compartments, whose borders were decorated by dense coverage of silver and gold colloidal grains. Anti-LAMP 1

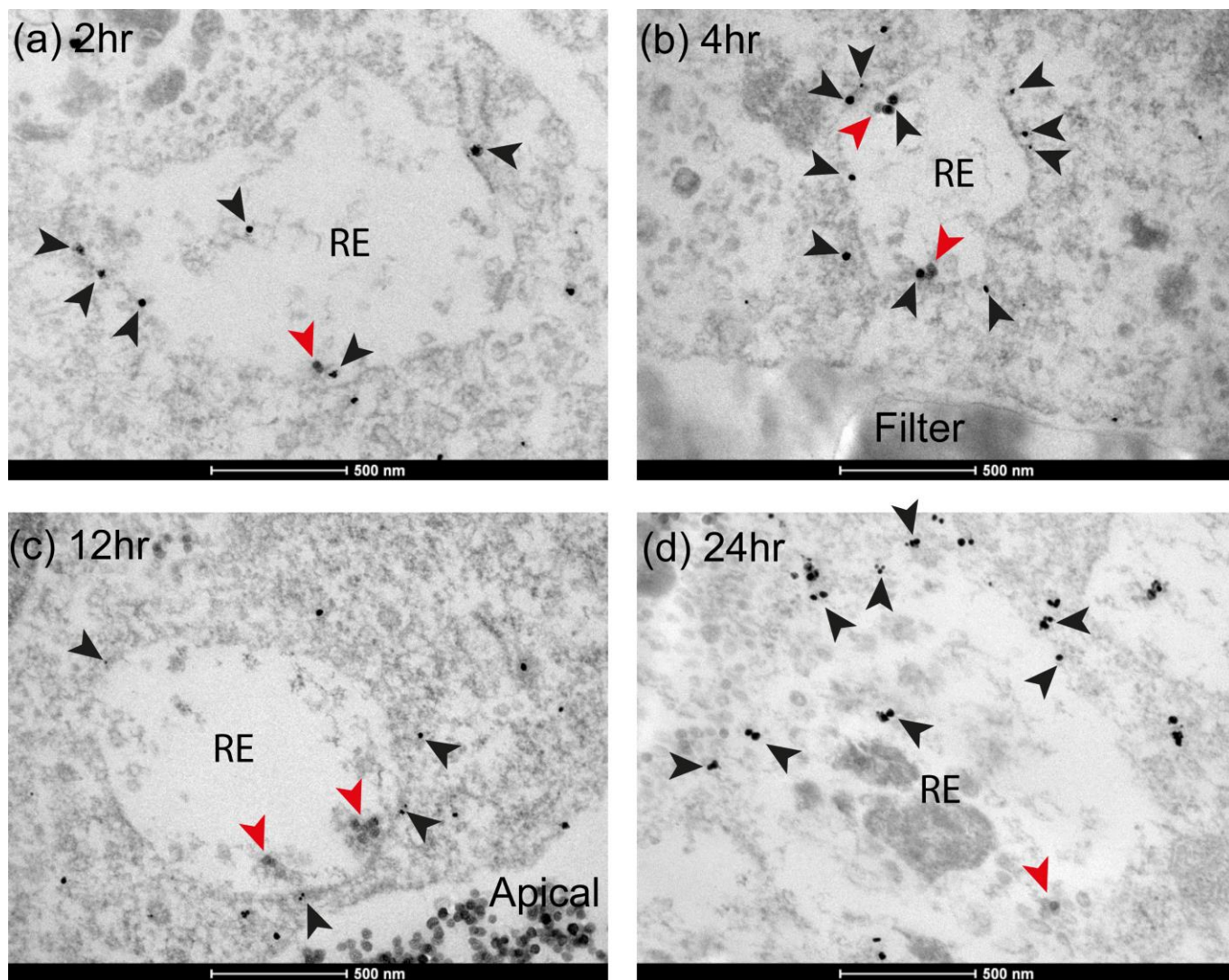immunostaining showed strong reactivity as well as high specificity.

Figure 3. Internalisation of 50 nm SiO_2-NPs in Rab 11-regulated recycling endosomes (RE) following exposure for 2, 4, 12 and 24 hours. The silver and gold colloidal grains and SiO_2-NPs were indicated with the black and red arrows respectively.

Biomolecules transported through the endo-lysosomal pathway have been reported to undergo export *via* recycling endosomes. The specific membrane regulator, Rab 11 mediates vesicle trafficking from early endosomes to the plasma membrane.[29] To verify if similar processes applied to nanoparticles, we labeled recycling endosomes with the Rab 11 antibody and subsequently nanogold-Fab' antibody. Similar to Rab 5 and Rab 7, the appearance of anti-Rab 7 IG particles was quantitatively less than EEA 1 or LAMP 1 staining, as seen by comparing Fig. 2 and Fig. 3. Overall, the epitope immunoreactivities of small Rab GTPase family proteins were lower in efficiency than other membrane-associated proteins such as EEA 1 or LAMP 1. The SiO_2-NPs were observed in small quantities in Rab11-stained endosomes, suggesting that although limited, recycling of silica nanoparticles to the plasma membrane is a potential pathway for exocytosis. The intracellular transport of nanoparticles seemed primarily to be controlled by the endo-lysosomal pathway, but we provided novel experimental evidence supporting transcytosis of nanoparticles across the BBB. Our IG electron microscopy demonstrated to be a novel and powerful approach to investigate trafficking of nanoparticles.
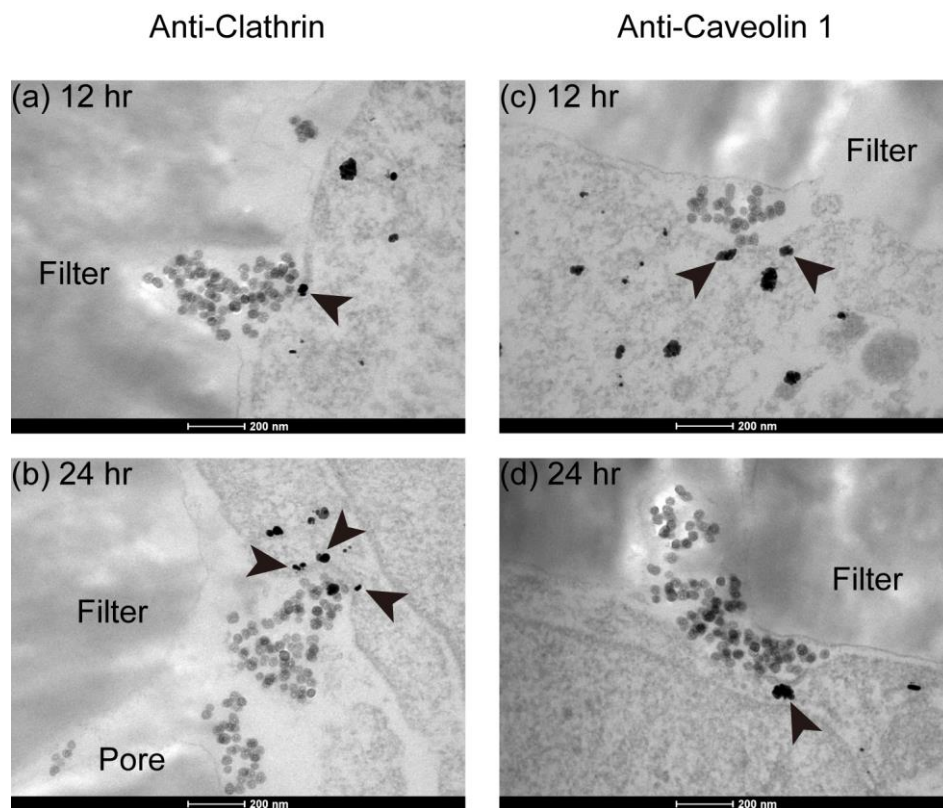
Anti-Clathrin   Anti-Caveolin 1

Figure 4. Anti-clathrin (a-b) and anti-caveolin 1 (c-d) IG examination to investigate the translocation of 50 nm SiO$_2$-NPs in the vicinity of the basal plasma membrane of the BBB after exposed for 24 and 12 hours respectively. Immunolocalisation of IG particles was indicated with the black arrows.

We previously reported accumulation and transcytosis of nanoparticles in the BBB, where the apical-to-basal trans-cellular transport was investigated with both fluorescence and electron microscopic imaging.[2, 26] As seen in Fig 4, SiO$_2$-NPs were translocated to the basal membrane of the BBB. NPs appeared to reside and form aggregates in the space between the filter and basal cell membrane. The BBB cell layer seemed to respond by organising the basal membrane surface to accumulate the nanoparticles into the pores of the transwell. In a polarized barrier, endocytosis might take place at the both apical and basolateral cell membrane.[39, 40] Herein, anti-clathrin and anti-caveolin 1 IG labeling were employed to reveal whether transcytosed nanoparticles underwent further endocytosis or a second uptake from the basolateral cell membrane of the BBB.

As described previously, clathrin and caveolin 1 are key actuators of endocytosis. Clathrin and caveolin 1 immunolabeling revealed potential endocytosis being initiated at the basolateral cell plasma membrane. After 12 and 24 hours of exposure, SiO$_2$-NPs were capped under omega-shape invaginations from the basal plasma membrane of the BBB cells. In Fig. 4a-b, IG particles were associated with the clathrin-dependent vesicles that were co-localised with SiO$_2$-NPs, suggesting that SiO$_2$-NPs were endocytosed at the basolateral side similarly to endocytosis observed on the apical side, as compared with Fig. 1a-c.

Potential secondary uptake of SiO$_2$-NPs via caveolin-mediated endocytosis was also investigated at the basal membrane. Caveolin, reportedly expressed in caveolae as well as elements

of secretory pathway,[35] played a role in mediating transcytosis of marcomolecules, such as albumin, transferrin, insulin, low-density lipoproteins (LDL) or chemokines etc.[41-44] Morphologically, caveolae are varied in size from 60-80 nm and have narrow and constricted necks around 10-50 nm.[36] However, SiO$_2$-NPs that accumulated between the basolateral membrane and the transwell filter formed clusters with a minimum size greater than 200 nm. As a result, caveolar vesicles were unlikely to mediate transcytosis of SiO$_2$-NPs aggregates at the basal membrane of the BBB. In Fig. 4c and d, the co-localisation between SiO$_2$-NPs and caveolae-stained vesicles were observed with basal membrane invaginations opening towards the filter. Although opening on a different side of cell membrane, the basal IG-labeled caveolae closely associated with SiO$_2$-NPs and displayed similar features in comparison with other apical caveolae-dependent structures (See Fig. 1d, e and f). Such re-entry activities might result from physical retention of SiO$_2$-NPs transported to the space between the basal membrane and the transwell membrane.

At the same time, some basal membrane invaginations that associated nanoparticles were found negative for both clathrin and caveolin immunolabeling, as shown in Supplementary Figure 4. In contrast to those positive immunolabels found in SF. 4d-f and 4j-l, the negative immunoreactive results (SF. 4a-c and 4g-i respectively) implicated there were different intracellular routing pathways utilised for export of SiO$_2$-NPs, not necessarily by clathrin or caveolin-mediated endocytic processes only as described above. More conclusive evidence is still needed to prove this case. Nevertheless, the literature reported that SiO$_2$-NPs could be exported by the BBB after

exposure of 4 hours.[26] Such transendothelial process might be linked with serial co-movements of vesicles, which could directly ferry cargos from one side to the other of the endothelial cell layer, without involving sorting and routing through the endo-lysosomal pathway.[45] In addition, there are also other rare pathways that can export nanoparticles. For example, lysosomes might fuse with the plasma membrane to initiate export of nanoparticles,[46, 47] in specific cell types as well as strict biological conditions (e.g., cell stress).[47, 48] Also, the recycling process of endosomes could be another export route that might contribute to the passage of nanoparticles, as observed in Fig. 3.

Conclusions

We applied the pre-embedding immunogold electron microscopic imaging, using nanogold-conjugated secondary antibodies, to examine different translocation sites of silica nanoparticles while crossing an *in vitro* human blood-brain barrier cell model. Apart from SiO_2-NPs, other nanoparticles for instance polystyrene could be also applied for this labeling approach, as it has suitable contrast with highly electron dense IG labels and compatibility with silver enhancement reagents. Our immunohistochemical permeablisation procedures allowed to retain the morphological integrity of cellular structures. The IG probes showed optimal penetration and accurate immunoreactivities with various target antigens in the BBB cells. Clathrin, caveolin 1, small GTPase Rab 5, 7, 11, EEA 1 and LAMP 1 proteins revealed through IG labels were used as markers for intracellular sorting and routing pathways of 50 nm SiO_2-NPs following their exposure at different times. Throughout the endo-lysosomal pathway, clathrin-dependent or independent endocytic vesicles, endosomes at various stages of maturation, as well as lysosomes were co-localised with SiO_2-NPs. In addition, Rab 11-labeled recycling endosomes were associated with SiO_2-NPs, suggesting a role of the recycling endosomes in exporting internalised silica nanoparticles. Moreover, after 12 and 24 hours of exposure, SiO_2-NPs were seen to reach the interface between the basal membrane and transwell filter, via potential transcytosis. By examining clathrin and caveolin 1 immunolabeling at the basolateral membrane, we discovered that although rare, the transcytosed SiO_2-NPs were able to re-enter the basal cell membrane via secondary endocytosis. In this study, we demonstrated that pre-embedding immunogold electron microscopic imaging was effective to overcome previous technical limitations and useful to provide a precise alternative to study the trans-cellular trafficking of nanoparticles within the BBB cells, allowing to unveil novel molecular mechanisms that govern endocytosis, exocytosis and transcytosis of nanoparticles across biological barriers.

Experimental

Materials and reagents

Cell culture flasks and transwells were purchased from Becton-Dickinson (BD, Ireland) and Corning Costar (Ireland) respectively. Cell culture medium EBM-2 and supplements (VEGF, IGF-1, EGF and basic FGF factors, hydrocortisone, ascorbate, gentamycin and 2 % fetal bovine serum) were all purchased from Lonza (Ireland). HEPES buffer and rat-tail type I collagen were acquired from Sigma-Aldrich (Ireland). 50 nm silica nanoparticles (SiO_2-NPs) were purchased from Kisher-

Biotech (www.kisher-biotech.com). LAMP 1 and EEA 1 antibodies were purchased from Abcam (www.abcam.com). Small GTPase Rab 5, 7 and 11 antibodies were obtained from Cell Signaling (www.cellsignal.com). Clathrin and caveolin 1 heavy chain antibodies were from Becton-Dickinson (BD, Ireland). Nanogold-Fab' fragment of anti-mouse or anti-rabbit IgG and HQ Silver Enhancement kit were purchased from Nanoprobes (NY, USA). Periodate-lysine-paraformaldehyde fixative (PLP) was prepared as described previously,[31] supplemented with 2 % formaldehyde, 0.01 M periodate, 0.075 M lysine and 0.075 M sodium phosphate buffer. Permeabilisation buffer (abbreviated as "Buffer" in this report) was prepared by mixing 0.01 % saponin and 0.1 % BSA in sodium phosphate buffer (100 mM, pH 7.4). Sodium phosphate buffer (100 mM) was prepared at pH 7.4. All these chemicals were obtained from Sigma Aldrich (Ireland).

Cell barrier culture

Immortalised human brain capillary microvascular endothelial cells (hCMEC/D3) were obtained from F. Miller and B. B. Weksler (INSERM, France). hCMEC/D3 cells used for the experiments were maintained between passage 25 and 35. The cells were cultured in EBM-2 complete medium (or growth medium) supplemented with VEGF, IGF-1, EGF, bFGF, 2.0 % FBS, ascorbate, gentamycin and hydrocortisone, as recommended by the manufacturer and literature.[49, 50] Before seeding the cells, transwell membranes were coated with rat-tail type I collagen for 30 min at 37 °C in a dry incubator and then rinsed with PBS once. hCMEC/D3 cells were seeded on coated transwell membranes (Polyester membrane, 12 well, pore size 0.4 µm, growth area 1.12 cm^2) at a density of 50,000 cells/well. For the barrier culture, the BBB cells were grown in a growth-factor depleted medium (or assay medium, consisting of EBM-2 supplemented with only bFGF, 2.5 % FBS, hydrocortisone, and 10 mM HEPES and gentamycine), as reported.[26, 51] The cells were then cultured in an incubator at 37 °C with 5 % CO_2, 95 % air and saturated humidity, and the assay medium was changed on the 4th and 7th days. The cell barriers were then immediately used.

Nanoparticle exposure

Before the exposure, the BBB cell barriers were rinsed with fresh assay medium. 50 nm SiO_2-NPs were freshly prepared with assay medium at a concentration of 100 µg/ml and measured with Dynamic Light Scattering (DLS) to ensure their dispersion at an optimal condition. After that, 0.5 ml 100 µg/ml SiO_2-NP solution was added to the top chambers of transwells, and 1.5 ml fresh assay medium to the bottom chambers. The barriers were then treated with SiO_2-NPs for 2, 4, 12 and 24 hours at a 37 °C incubator with 5 % CO_2, 95 % air and saturated humidity.

Immunogold labeling

All labeling procedures were carried out at room temperature unless otherwise stated. Before the immunostaining, the BBB barriers were rinsed with PBS for three times to remove remaining nanoparticles from the top and bottom chambers of transwells. The barriers were incubated with PLP fixative (as described before) for 2 hours. Following three washes of 0.1 M sodium phosphate buffer, samples were permeabilised with Buffer for 8 min (as described before). Each primary antibody (mouse or rabbit IgG) was introduced independently and

incubated for 1 hour with a recommended dilution according to the antibody supplier. After three washes with Buffer, 1.4 nm nanogold-Fab' goat anti-mouse or anti-rabbit IgG (1:50 dilution) was applied according to the origin of the primary antibody and incubated for another hour. Excess antibody was washed for three times with Buffer, and then with sodium phosphate buffer. Samples were then post-fixed with 1 % glutaraldehyde for 10 min, washed and quenched with 50 mM Glycine for 5 min. In order to improve electron visibility of immunogold particles, silver enhancement was performed using HQ SILVER ™ Enhancement kit, as instructed by Nanoprobes (NY, USA). Briefly, the initiator was first dispensed into a clean tube, and added by the moderator, and then the activator. The three components were used at an equal amount. Size development for the silver and gold colloidal grains was optimised by using different silver-developing times in order to acquire the optimal visibility for immunogold particles under TEM. In this report, we used 5-7 min development time.

Transmission electron microscopy

After completion of the immunolabeling procedures, the BBB cell barriers were fixed with or without glutaraldehyde (2.5 %, v/v) in Sorensen's phosphate buffer for 1 hour at room temperature. Samples were briefly rinsed, with Sorensen's phosphate buffer, post-fixed in osmium tetroxide (1 %, w/v) for 1 hour, and rinsed again with Sorensen's phosphate buffer. The barrier samples were dehydrated in a graded ethanol series (30 %, 50 % 70 %, 90 % and 100 %). When dehydration was complete samples were transferred from 100 % ethanol to an ethanol/epon resin mixture (1:1 v/v) for 1 hour. To complete resin infiltration the samples were transferred to pure epon resin for 2 hours at 37 °C. The final polymerization was performed at 60 °C for 24 hours. Ultrathin sections (80 nm) were cut with a diamond knife (DiATOME, USA) and further stained with 2 % uranyl acetate for 20 min and 0.4 % lead citrate for 10 min. Sections were imaged with a transmission electron microscope (TECNAI G^2 BioTWIN, FEI Company, USA) using an accelerating voltage of 120 kV.

Acknowledgements

Notes and references

* Corresponding author: kenneth.a.dawson@cbni.ucd.ie
[1] Centre for BioNano Interactions, School of Chemistry and Chemical Biology, University College Dublin, Belfield, Dublin 4, Ireland.
[2] UCD Conway Institute of Biomolecular and Biomedical Research, University College Dublin, Belfield, Dublin 4, Ireland.

† Electronic Supplementary Information (ESI) available: Nanoparticle characterisation data, preservation of cellular structures, staining controls, optimisation of size amplification *via* the silver enhancement, and more imaging results from anti-clathrin and anti-caveolin 1 immunolabeling. See DOI: 10.1039/b000000x/

1. Sandin, P.; Fitzpatrick, L. W.; Simpson, J. C.; Dawson, K. A. *ACS Nano* **2012,** 6, (2), 1513-21.

2. Bramini, M.; Ye, D.; Hallerbach, A.; Raghnaill, M. N.; Salvati, A.; Åberg, C.; Dawson, K. A. *ACS Nano* **2014,** 8, (5), 4304-4312.

3. Huang, B.; Bates, M.; Zhuang, X. *Annual Review of Biochemistry* **2009,** 78, 993-1016.

4. Pavani, S. R. P.; Thompson, M. A.; Biteen, J. S.; Lord, S. J.; Liu, N.; Twieg, R. J.; Piestun, R.; Moerner, W. *Proceedings of the National Academy of Sciences* **2009,** 106, (9), 2995-2999.

5. Fernandez-Suarez, M.; Ting, A. Y. *Nat Rev Mol Cell Biol* **2008,** 9, (12), 929-943.

6. Betzig, E.; Patterson, G. H.; Sougrat, R.; Lindwasser, O. W.; Olenych, S.; Bonifacino, J. S.; Davidson, M. W.; Lippincott-Schwartz, J.; Hess, H. F. *Science* **2006,** 313, (5793), 1642-1645.

7. Rust, M. J.; Bates, M.; Zhuang, X. *Nature Methods* **2006,** 3, (10), 793-796.

8. Nieuwenhuizen, R. P.; Lidke, K. A.; Bates, M.; Puig, D. L.; Grünwald, D.; Stallinga, S.; Rieger, B. *Nature Methods* **2013,** 10, (6), 557-562.

9. Amiry-Moghaddam, M.; Ottersen, O. P. *Nature Neuroscience* **2013,** 16, (7), 798-804.

10. Berryman, M. A.; Rodewald, R. D. *Journal of Histochemistry & Cytochemistry* **1990,** 38, (2), 159-170.

11. Yi, H.; Leunissen, J. L.; Shi, G. M.; Gutekunst, C. A.; Hersch, S. M. *Journal of Histochemistry & Cytochemistry* **2001,** 49, (3), 279-283.

12. Bouchet-Marquis, C.; Hoenger, A. *Micron* **2011,** 42, (2), 152-162.

13. Bergles, D. E.; Roberts, J. D. B.; Somogyi, P.; Jahr, C. E. *Nature* **2000,** 405, (6783), 187-191.

14. Tanner, V. A.; Ploug, T.; Tao-Cheng, J. H. *Journal of Histochemistry & Cytochemistry* **1996,** 44, (12), 1481-1488.

15. Burry, R.; Vandre, D.; Hayes, D. *Journal of Histochemistry & Cytochemistry* **1992,** 40, (12), 1849-1856.

16. Viall, C. A.; Holloway, H.; Chen, Q.; Stone, P. R.; Chamley, L. W. *Placenta* **2014,** 35, (3), 223-227.

17. Bos, E.; Hussaarts, L.; van Weering, J. R. T.; Ellisman, M. H.; de Wit, H.; Koster, A. J. *J Struct Biol* **2014,** 186, (2), 273-282.

18. Liu, J.; Yu, M.; Zhou, C.; Yang, S.; Ning, X.; Zheng, J. *Journal of the American Chemical Society* **2013,** 135, (13), 4978-81.

19. Anguissola, S.; Garry, D.; Salvati, A.; O'Brien, P. J.; Dawson, K. A. *PloS one* **2014,** 9, (9), e108025.

20. Kim, J. A.; Åberg, C.; Salvati, A.; Dawson, K. A. *Nature Nanotechnology* **2012,** 7, (1), 62-68.

21. Lesniak, A.; Fenaroli, F.; Monopoli, M. P.; Åberg, C.; Dawson, K. A.; Salvati, A. *ACS Nano* **2012,** 6, (7), 5845-5847.

Nanoscale Accepted Manuscript

22. Santos, T.; Varela, J.; Lynch, I.; Salvati, A.; Dawson, K. A. *Small* **2011,** 7, (23), 3341-3349.

23. Shapero, K.; Fenaroli, F.; Lynch, I.; Cottell, D. C.; Salvati, A.; Dawson, K. A. *Mol Biosyst* **2011,** 7, (2), 371-378.

24. Salvati, A.; Aberg, C.; dos Santos, T.; Varela, J.; Pinto, P.; Lynch, I.; Dawson, K. A. *Nanomedicine* **2011,** 7, (6), 818-26.

25. Salvati, A.; Pitek, A. S.; Monopoli, M. P.; Prapainop, K.; Bombelli, F. B.; Hristov, D. R.; Kelly, P. M.; Aberg, C.; Mahon, E.; Dawson, K. A. *Nat Nanotechnol* **2013,** 8, (2), 137-43.

26. Ye, D.; Raghnaill, M. N.; Bramini, M.; Mahon, E.; Åberg, C.; Salvati, A.; Dawson, K. A. *Nanoscale* **2013,** 5, 11153-11165.

27. Elsaesser, A.; Barnes, C. A.; McKerr, G.; Salvati, A.; Lynch, I.; Dawson, K. A.; Howard, C. V. *Nanomedicine : Nanotechnology, Biology, and Medicine* **2011,** 6, (7), 1189-1198.

28. Elsaesser, A.; Taylor, A.; de Yanés, G. S.; McKerr, G.; Kim, E.-M.; O'Hare, E.; Howard, C. V. *Nanomedicine : Nanotechnology, Biology, and Medicine* **2010,** 5, (9), 1447-1457.

29. Stenmark, H. *Nat Rev Mol Cell Biol* **2009,** 10, (8), 513-525.

30. Griffiths, G., Fixation for fine structure preservation and immunocytochemistry. In *Fine Structure Immunocytochemistry*, Springer: 1993; pp 26-89.

31. McLean, I. W.; Nakane, P. K. *Journal of Histochemistry & Cytochemistry* **1974,** 22, (12), 1077-1083.

32. Hayat, M. A. *Micron and Microscopica Acta* **1986,** 17, (2), 115-135.

33. Ye, D.; Dawson, K. A.; Lynch, I. *The Analyst* **2014**.

34. Le Roy, C.; Wrana, J. L. *Nat Rev Mol Cell Biol* **2005,** 6, (2), 112-126.

35. Li, W. P.; Liu, P.; Pilcher, B. K.; Anderson, R. *J Cell Sci* **2001,** 114, (7), 1397-1408.

36. Wang, Z.; Tiruppathi, C.; Minshall, R. D.; Malik, A. B. *ACS Nano* **2009,** 3, (12), 4110-4116.

37. McMahon, H. T.; Boucrot, E. *Nat Rev Mol Cell Biol* **2011,** 12, (8), 517-533.

38. Sabella, S.; Carney, R. P.; Brunetti, V.; Malvindi, M. A.; Al-Juffali, N.; Vecchio, G.; Janes, S. M.; Bakr, O. M.; Cingolani, R.; Stellacci, F. *Nanoscale* **2014,** 6, (12), 7052-7061.

39. Apodaca, G. *Traffic* **2001,** 2, (3), 149-159.

40. von Bonsdorff, C. H.; Fuller, S. D.; Simons, K. *The EMBO Journal* **1985,** 4, (11), 2781-2792.

41. Ghitescu, L.; Fixman, A.; Simionescu, M.; Simionescu, N. *J Cell Biol* **1986,** 102, (4), 1304-1311.

42. Soda, R.; Tavassoli, M. *J Ultrastruct Res* **1984,** 88, (1), 18-29.

43. King, G. L.; Johnson, S. M. *Science* **1985,** 227, (4694), 1583-6.

44. Ge, S.; Song, L.; Serwanski, D. R.; Kuziel, W. A.; Pachter, J. S. *J Neurochem* **2008,** 104, (5), 1219-32.

45. Tuma, P. L.; Hubbard, A. L. *Physiological Reviews* **2003,** 83, (3), 871-932.

46. Luzio, J. P.; Pryor, P. R.; Bright, N. A. *Nat Rev Mol Cell Biol* **2007,** 8, (8), 622-632.

47. Yanes, R. E.; Tarn, D.; Hwang, A. A.; Ferris, D. P.; Sherman, S. P.; Thomas, C. R.; Lu, J.; Pyle, A. D.; Zink, J. I.; Tamanoi, F. *Small* **2013,** 9, (5), 697-704.

48. Serpooshan, V.; Mahmoudi, M. *Advances in Colloid and Interface Science* **2013,** 201-202, 18-29.

49. Poller, B.; Gutmann, H.; Krahenbuhl, S.; Weksler, B.; Romero, I.; Couraud, P. O.; Tuffin, G.; Drewe, J.; Huwyler, J. *Journal of Neurochemistry* **2008,** 107, (5), 1358-68.

50. Weksler, B. B.; Subileau, E. A.; Perriere, N.; Charneau, P.; Holloway, K.; Leveque, M.; Tricoire-Leignel, H.; Nicotra, A.; Bourdoulous, S.; Turowski, P.; Male, D. K.; Roux, F.; Greenwood, J.; Romero, I. A.; Couraud, P. O. *FASEB Journal* **2005,** 19, (13), 1872-4.

51. Nic Raghnaill, M.; Brown, M.; Ye, D.; Bramini, M.; Callanan, S.; Lynch, I.; Dawson, K. A. *Eur J Pharm Biopharm* **2011,** 77, (3), 360-7.

Nanoscale Accepted Manuscript